Applied Nanoscience (2020) 10:95–105
https://doi.org/10.1007/s13204-019-01049-7

ORIGINAL ARTICLE

Nano-electrokinetic ion enrichment in a micro-nanofluidic preconcentrator with nanochannel's Cantor fractal wall structure

Wenbo Han[1] · **Xueye Chen**[1]

Received: 19 March 2019 / Accepted: 2 May 2019 / Published online: 10 May 2019

Abstract

The detection of ultra-low concentration of biomacromolecules remains the focus of research in micro-nanofluidic systems. Sample enrichment is primarily targeted at very low concentration of sample detection tasks. The use of ion concentration polarization principle is the most efficient means to solve the problem of electrokinetic ion enrichment. In this paper, numerical simulation of nano-electrokinetic ion enrichment in a micro-nanofluidic preconcentrator with nanochannel's Cantor fractal wall structure was performed based on Poisson–Nernst–Planck equation combined with the Navier–Stokes equation. The results show that reducing the initial length L_0, increasing the initial height h_0, increasing the fractal step n and using the unstaggered structure in the Cantor fractal principle can increase the ion enrichment concentration and peak voltage. The initial ion concentration is 0.1 mol/m^3. When the applied voltage is 30 V and the initial height h_0 increases from 35 to 45 nm, the ion enrichment concentration drastically increases from 1.007 to 1.410 mol/m^3 by 40%. This study provides a theoretical basis and a novel design method for improving the sensitivity of micro-nanofluidic chips and the design of ultra-low concentration sample testing equipment.

Keywords Nano-electrokinetic ion enrichment · Nanofluidics · Cantor fractal principle · ICP · PNP

List of symbols

x	Horizontal coordinate
y	Vertical coordinate
l_1	Microchannel length
l_2	Nanochannel length
d_1	Microchannel width
d_2	Nanochannel width
L_0	Initial length in Cantor fractal principle
h_0	Initial height in Cantor fractal principle
X	Number of asperities on a repeating segment
n	Fractal step
N	Number of ion species in solution
e	Elementary charge
p	Pressure
j	Species flux
u	Fluid velocity
D_k	Ion diffusion coefficient
z_k	The valence of the kth ion
n_k	Concentration of the kth ion

Greek symbols

ϕ	Potential
ρ_e	Volumetric charge density
ε_0	Electrical permittivity of the vacuum
ε_r	Relative permittivity
ρ_0	Fluid density
μ	Dynamic viscosity of fluid
ω_k	Electrophoretic mobility

Subscripts/superscripts

k	The kth species
$+$	Positive mono-valence
$-$	Negative mono-valence
$\perp$	Normal component

Introduction

With the improvement of micro-nano manufacturing technology, nanotechnology has been widely used in many fields, such as the rheology of complex liquids (Mozaffari et al. 2017), the dynamics of petroleum and fracturing fluids (Hasham et al. 2018), nanomedicine (Amoyav and Benny 2018) and so on. Micro-nanofluidic chip technology is a technique for performing micro-analytical chemistry and

✉ Xueye Chen
xueye_chen@126.com

[1] Faculty of Mechanical Engineering and Automation, Liaoning University of Technology, Jinzhou 121001, China

biological experiments by operating tiny fluids in micro-nano channels (Wang et al. 2016; Shi et al. 2018; Shi et al. 2018). Tasks such as sample preparation, enrichment, separation, collection, and detection are often performed on microfluidic chips (Lin et al. 2011; Wang and Han 2008). However, the concentration of most biomolecules in biological samples is very low, some proteins are as low as pmol/L. It is much lower than the detection ranges of traditional test equipment, which greatly limits the completion of detection tasks (Jia et al. 2010). To solve this critical problem, in addition to developing new detection techniques and improving equipment accuracy, nanofluidic nanoelectrokinetic ion enrichment methods can also be used (Wu and Steckl 2009; Lee et al. 2007). Therefore, researchers are now paying more and more attention to ion and particle transport in nanochannels (Srinivasacharya and Surender 2015; Ali et al. 2019). Nanofluids generally refer to the study of fluid behavior in channels less than 100 nm in size (Whitesides 2006; Eijkel and Van Den Berg 2005). The nanochannels have a large specific surface area, which leads to an increase in the electrical resistance of the fluid in the nanochannel and an overlap of the electric double layer (Plecis et al. 2005). Nanochannels have unparalleled advantages. For example, basic research at the single molecule level is not possible in microchannels and can be performed in nanochannels (Rissin et al. 2010). At present, nanofluids have been applied to the separation of biological macromolecules (Cabodi et al. 2002), molecular enrichment (Kim and Han 2008), seawater desalination (Kim et al. 2010) and capacity collection (van der Heyden et al. 2007).

In the nanofluidic study, the most efficient way to achieve electrokinetic ion enrichment is to use the principle of ICP (Li and Anand 2016). The principle of ICP is to realize the electrokinetic ion enrichment by forming the enrichment region in the micro-nanochannel and utilizing the unique selective transmission principle of the overlapping electric double layer in the nanochannel (Daiguji et al. 2004). To achieve ultra-low concentration molecular detection, research on electrokinetic ion enrichment was carried out. Pu et al. first demonstrated the enrichment and depletion of ions on both ends of negatively charged glass nanochannels and theoretically explained the concentration polarization phenomenon (Pu et al. 2004). Jia et al. demonstrated that the high electrophoretic mobility (EPM) of the counterion in the membrane plays the most important role in numerical simulation (Jia and Kim 2014). MacDonald et al. proposed a scalable out-of-plane desalination method using ion concentration polarization and find that energy efficiency is not sensitive to flow rate (MacDonald et al. 2014). Wang et al. showed that the enrichment stability can be improved by increasing the microchannel width, reducing the microchannel length and reducing the surface charge density Wang et al. (2016). Gong et al. proposed a novel ion concentration polarized microfluidic device for the continuous extraction of Li + from high Mg2 +/Li + ratio brines (Gong et al. 2018). Lin et al. found that the regeneration of pores is caused by the presence of high density surface charges and high migration hydroxide ions (Lin et al. 2018). Gao and Liu et al. studied the enrichment and enrichment separation of ions on paper-based chips by experimental methods (Gao et al. 2018; Liu et al. 2019).

In general, it is important to study the theory of electrokinetic ion enrichment. Because electrokinetic ion enrichment theory has a guiding significance for improving the detection ability of ultra-low concentration and the sensitivity of micro-nanofluidic chips. However, most of the current research focuses on straight line nanochannels and little research has been done on the design and fabrication of complex structures of the nanochannel wall (Movahed and Li 2011; Silber-Li et al. 2012). Therefore, it is necessary to design the complex structure of the nanochannel wall.

In this paper, nano-electrokinetic ion enrichment in a micro-nanofluidic preconcentrator with nanochannel's Cantor fractal wall structure has been studied by numerical simulation based on the Poisson–Nernst–Planck equation and the Navier–Stokes equation. The numerical model is presented in the Sect. 2. The effects of initial length L_0, initial height h_0, fractal step n and staggered structure on electrokinetic ion enrichment in the Cantor fractal principle are discussed in the Sect. 3. Finally, a conclusive summary is presented.

Methodology

The numerical simulation of this work is based on the finite element software *COMSOL Multiphysics*®. To study nano-electrokinetic ion enrichment in a micro-nanofluidic preconcentrator with nanochannel's Cantor fractal wall structure, a set of coupled partial differential equations are solved, including the Poisson equation, the Nernst–Planck equation and the Navier–Stokes equation (Wang et al. 2009).

To ensure the accuracy of numerical calculations, we made the following assumptions about the ionization, molecular volume and collision and solution permittivity of water molecules in the simulation:

- The ionization of water molecules is not considered.
- The volume of ions is ignored.
- The interaction between ions, ions and water molecules is ignored.
- The permittivity in the liquid phase is the same everywhere.

- Under these assumptions, we have established a mathematical model and conducted numerical simulation analysis.

Governing equations

Electric field

The Poisson equation (Eq. 1) is applied to solve the distribution of the electrical potential. The distribution of the electrical potential depends mainly on the applied voltage and surface charge. According to Eq. 2, the electric field strength is solved by solving the gradient of the electrical potential.

$$\nabla \cdot \left(\varepsilon_r \varepsilon_0 \nabla \phi\right) = -\sum_{k=1}^{N} e z_k n_k \tag{1}$$

$$E = -\nabla \phi \tag{2}$$

The surface electric charge density is used as a boundary condition. The surface electric charge density is set to 0 V in Eq. 3. The electric potential is used as another boundary condition. In Eq. 4, the electric potential is set as positive voltage and 0 voltage.

$$-n \cdot \varepsilon_0 \varepsilon_r E = \sigma_0 \tag{3}$$

$$\phi = \phi_0 \tag{4}$$

Ionic concentration field

As shown in Eq. 5, the Nernst–Planck equation was used to simulate ion transport and ion concentration distribution which depended on the electrophoresis, electroosmosis and diffusion in the micro-nano composite channel.

$$\frac{\partial n_k}{\partial t} + \nabla \cdot \left(-\omega_k z_k n_k \nabla \phi\right) - \nabla \cdot \left(D_k \nabla n_k\right) + \nabla \cdot \left(n_k u\right) = 0 \tag{5}$$

In Eq. 6, the constant ion concentration is set to 0.1 mol/m^3. In Eq. 7, the micro-nano composite channel is set to be impermeable to ions.

$$c = c_0 \tag{6}$$

$$n \cdot \left(-\omega_k z_k n_k \nabla \phi - D_k \nabla n_k + n_k u\right) = 0 \tag{7}$$

Flow field

The incompressible Navier–Stokes equation (Eq. 8) with electrical force ($-\rho_e \nabla \phi$) and the continuity equation (Eq. 9) are used to describe the flow field. This means that the density of the fluid is always constant.

$$\rho_0\left(\partial_t u + u \cdot \nabla u\right) = -\nabla p + \mu \nabla^2 u - \rho_e \nabla \phi \tag{8}$$

$$\nabla \cdot u = 0 \tag{9}$$

Pressure is set as a boundary condition. In Eq. 10, the inlet and outlet pressures are set to 0 Pa, respectively. In Eq. 11, the micro-nano composite channel is set to have no slip boundary condition.

$$P = P_0 \tag{10}$$

$$u = 0 \tag{11}$$

Simulation setup

To study the effect of the nanochannel with Cantor fractal wall structure on electrokinetic ion enrichment, we designed a two-dimensional numerical simulation model. A schematic diagram of the numerical model is shown in Fig. 1. Since the wall structure of the nanochannel is more complicated, we show a schematic diagram of the wall structure of the nanochannel in Fig. 2. It is depicted in Fig. 1 that the micro-nano preconcentrator consists of two microchannels and one nanochannel vertically connected to the microchannels. The length and width of the microchannels are $l_1 = 3$ μm and $d_1 = 1$ μm, respectively.

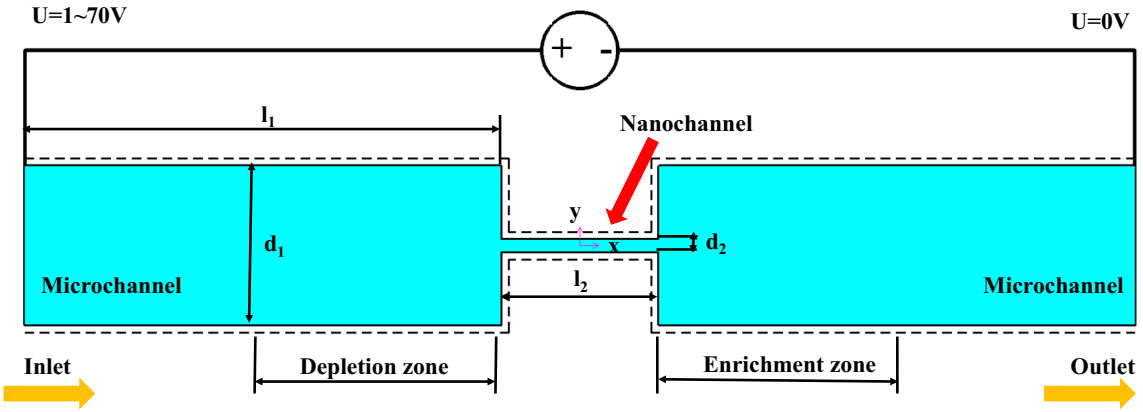

Fig. 1 2D numerical model diagram

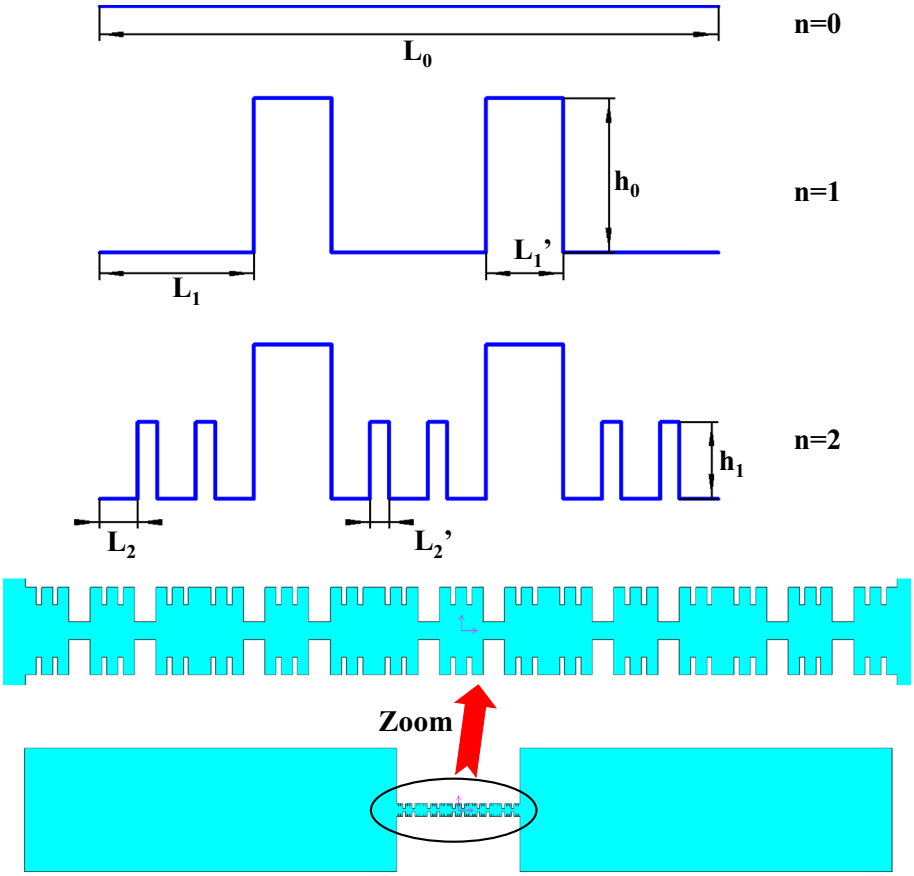

Fig. 2 Cantor fractal principle and the basic structure S0

The length and width of the nanochannels are $l_2 = 1$ μm and $d_2 = 0.1$ μm. An external voltage is applied across the two microchannels. The applied voltage on the left side is 1–70 V, and the applied voltage on the right side is 0 V. Based on the Cantor fractal principle, the wall surface of the nanochannel is structurally designed (Chen et al. 2010). Figure 2 shows the Cantor fractal principle and the design of the nanochannel wall structure based on Cantor fractal principle. Based on the Cantor fractal principle, we have designed a variety of different wall structures. The wall structure shown in Fig. 2 is called the basic structure S0. As shown in Fig. 2, the following steps are the wall structure generation steps based on the Cantor fractal principle:

1. In the horizontal direction, the 0th line segment is divided into 2X-1 segments. The odd-numbered segments are equal in length to the odd-numbered segments, and the even-numbered segments are equal in length to the even-numbered segments. In the vertical direction, the even height of the even number of segments is h_0;
2. According to the above method, each odd segment is subdivided into 2X-1 segments, wherein the even segment height is 1/2 of the previous height h_0.

We conclude that the wall structure design formula based on the Cantor fractal principle is as follows,

$$L_n = \left(\frac{1}{f_x}\right)^n * L_0 \tag{12}$$

$$h_n = \left(\frac{1}{f_z}\right)^n * h_0 \tag{13}$$

In this paper, $f_x = 4$, $f_z = 2$. As shown in Fig. 2, the dimensions in the basic structure S0 are, respectively, $L_0 = 200$ nm, $L_1 = 50$ nm, $L_1' = 25$ nm, $L_2 = 6.25$ nm, $L_2' = 3.125$ nm, $h_0 = 40$ nm and $h_1 = 20$ nm. The temperature in the system remains unchanged at 293.15 K. In this paper, potassium chloride (KCl) can be completely disassociated into K^+ ions and Cl^- ions in aqueous solution. Detailed ion physical parameters are shown in Table 1. The boundary conditions of the two-dimensional geometric model are shown in Table 2. The mesh

Table 1 The value of the ion parameter in the simulation

ρ_0(kg/m^3)	ε_0(F/m)	ε_r	D_1/D_2(m^2/s)	μ(Pa·s)	z_1/z_2
1.0×10^3	8.85×10^{-12}	80	$1.97\times10^{-9}/2.01\times10^{-9}$	1.0×10^{-3}	1/−1

Table 2 Boundary conditions of the model in the simulation

	Inlet and outlet	The wall of the microchannel	The wall of the nanochannel
Electric field	$\phi_{inlet}=1$–70 V, $\phi_{outlet}=0$ V	$\sigma_{micro}=-8e^{-4}C/m^2$	$\sigma_{nano}=-8e^{-4}C/m^2$
Ionic field	$c_{inlet}=c_{outlet}=0.1$ mol/m^3	$j_{\perp}=0$	$j_{\perp}=0$
Flow field	$p=0$ Pa	$u=0$	$u=0$

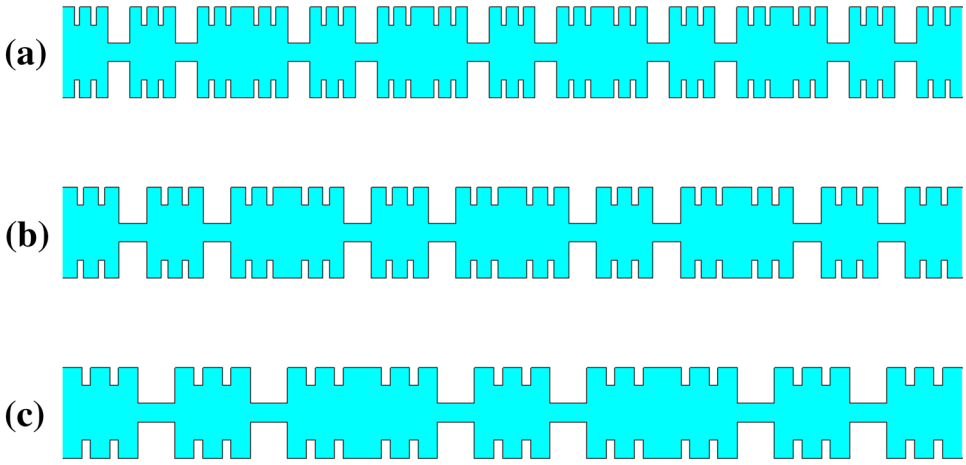

Fig. 3 Design of nanochannel wall structure with three different initial length L_0 based on Cantor fractal principle. **a** $L_0=200$ nm, **b** $L_0=250$ nm, **c** $L_0=333.33$ nm

in the nanochannel is 5 nm and the mesh in the microchannel is 50 nm. By increasing the number of grids, reliable results with no change can be obtained.

Results and discussion

Effects of initial length L_0 on ion enrichment

It is focused on the effect of the initial length L_0 in the Cantor fractal principle on ion enrichment. In this section, all other parameters (such as the applied voltage, and the fluid parameters) in the basic structure *S*0 are kept unchanged and only the initial length L_0 is changed. As shown in Fig. 3, L_0 in Fig. 3a, b, c are 200 nm, 250 nm and 333.33 nm, respectively. Figure 3a is the basic structure *S*0. To study the peak concentration and the peak voltage of different structures, an applied voltage of 1–70 V was applied across the microchannels. The peak concentration curve for the three different Cantor fractal nanochannels is plotted as shown in Fig. 4. From Fig. 4, when the initial length L_0 in the Cantor fractal principle is increased from 200 to 333.33 nm, the ion peak concentration decreases from 1.152 to 1.025 mol/m^3 and the peak voltage decreases from 36 to 29 V. Previous study has shown that electrokinetic ion enrichment is mainly due to the balance between the electrophoresis force generated by the electrophoresis effect and the repulsion of surface charge (Wang et al. 2013). To further explain the influence of the initial length L_0 on ion enrichment in the Cantor fractal principle, we obtained the concentration diagram as shown

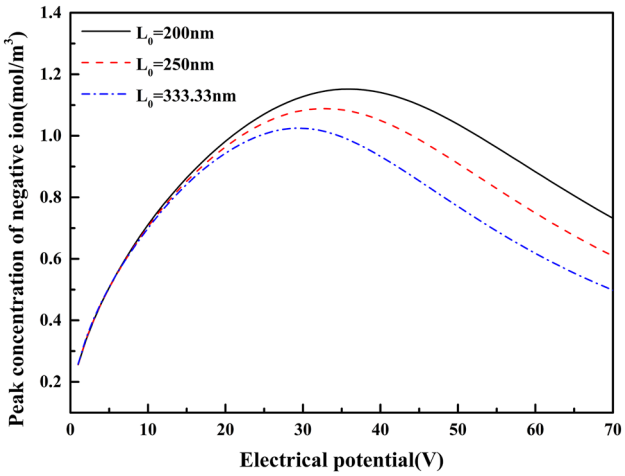

Fig. 4 Ion peak concentration curve for three different initial length L_0

in Fig. 5 when the applied voltage is 30 V. In Fig. 5a, b, c the arrows represent only the direction of velocity and do not represent the magnitude of the velocity. It is clear from Fig. 5a, b, c that two distinct vortex flows are produced in the depletion zone. This is due to the lower concentration of the depletion zone where the local electric field is significantly amplified and resulting in a vortex flow that forms the ICP. When L_0 increases from 200 to 333.33 nm, the unit structure of the Cantor fractal is significantly increased and the number of Cantor fractal units on the wall is significantly reduced. The smaller the number of Cantor fractal units, the

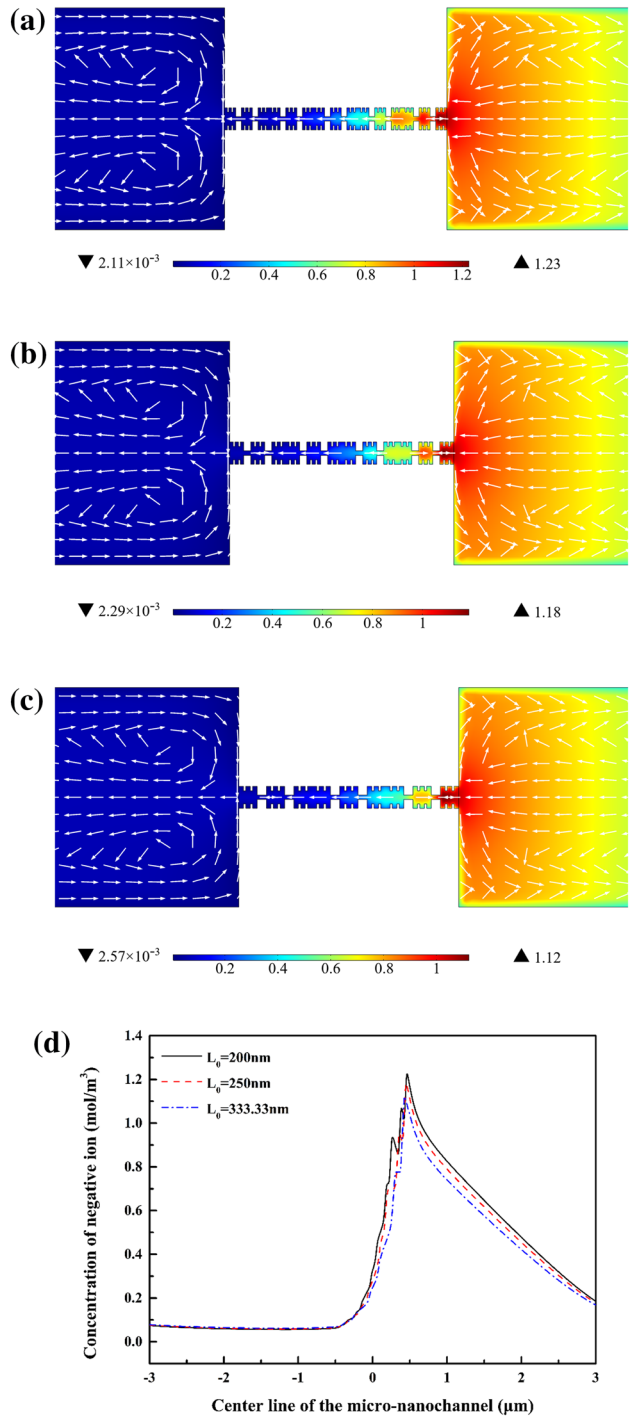

Fig. 5 Ion concentration image of three different initial length L_0 at an applied voltage of 30 V and ion concentration curve at the center line of the micro-nanochannel. **a** L_0 = 200 nm, **b** L_0 = 250 nm, **c** L_0 = 333.33 nm

more the electric double layer overlap in the nanochannels. Therefore, the more the number of units, the stronger the repulsive force it has. It requires a higher voltage to provide an electrophoresis effect to balance the repulsion effect of the electric double layer. However, when L_0 is reduced from 333.33 to 200 nm as shown in Fig. 4, the peak voltage is only increased by 7 V, while the peak concentration of ions is increased by 12%. This is a distinct advantage in that it consumes very little power and significantly increases the peak concentration of ions. As shown in Fig. 5d, the ion concentration curve at the center line of the micro-nanochannel is at the applied voltage of 30 V. As is clear from Fig. 5d, the smaller the initial length L_0 in the Cantor fractal principle, the higher the ion concentration of the enrichment zone. It is proved that the smaller the initial length L_0 in the Cantor fractal principle is, the higher the overlap of its electric double layer is, and the stronger the repulsive force is. It causes the anions not to pass through the nanochannels and form an enrichment phenomenon in the enrichment zone.

Furthermore, we found that the initial length L_0 in the Cantor fractal principle has a significant impact on ion enrichment. Decreasing the initial length L_0 of the Cantor fractal can significantly increase the peak concentration of electrokinetic ion enrichment. When the initial length L_0 becomes smaller, there will be more Cantor fractal units on the wall which poses a challenge to today's micro-nano manufacturing technology. It will drive the development of micro-nano manufacturing technology.

Effects of initial height h_0 on ion enrichment

To study the effect of the initial height h_0 in the Cantor fractal principle on the ion enrichment, we designed three different initial heights of the Cantor fractal wall structure. Only the initial height h_0 is changed and the other parameters of the basic structure *S*0 remain unchanged. The h_0 values in Fig. 6a, b, c are 35 nm, 40 nm and 45 nm, respectively. A peak concentration curve as shown in Fig. 7 is plotted by applying a voltage of 1–70 V to both ends of the microchannels. It is found from Fig. 7 that the peak voltage is increased from 30 to 52 V and the peak concentration is increased by 40% when the initial height h_0 is increased from 35 to 45 nm. It is indicated that the initial height h_0 has the most significant effect on the peak concentration of electrokinetic ion enrichment. To further explain the effect of the initial height h_0 in the Cantor fractal principle on the ion enrichment, an ion concentration image was plotted as shown in Fig. 8 at an applied voltage of 30 V. As seen from Fig. 8a, b, c, when the initial height h_0 is increased, a part of the nanochannel is significantly narrowed. Narrowing of the nanochannel increases the overlap of the electric double layer. The larger the initial height h_0, the stronger the overlap of the electric double layer, and the stronger the repulsive force it has. So it requires a higher peak voltage to provide an electrophoresis effect to balance the repulsive force. As the initial height h_0 increases, the ion concentration of the enrichment zone increases and the concentration

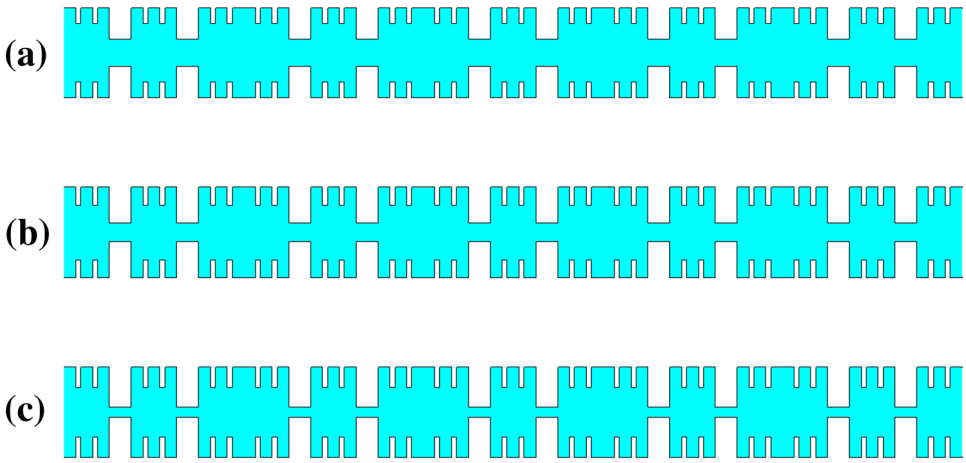

Fig. 6 Design of nanochannel wall structure with three different initial height h_0 based on Cantor fractal principle. **a** $h_0=35$ nm, **b** $h_0=40$ nm, **c** $h_0=45$ nm

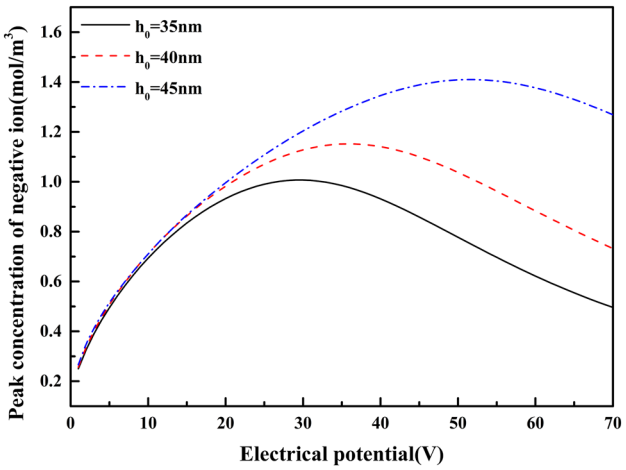

Fig. 7 Ion peak concentration curve for three different initial height h_0

of the depletion zone decreases which is shown in Fig. 8d. It is shown that the higher the initial height h_0, the weaker the electrophoresis effect of the enrichment region when the voltage is constant. The ions cannot pass through the nanochannel and the concentration in the enrichment zone will increase. However, the lower the initial height h_0, the lower the repulsive force of the electric double layer it possesses. Due to the electrophoresis effect, ions will reach the depletion region through the nanochannel and the concentration in the depletion region will increase. Based on previous studies and our analysis, we believe that the factors affecting the ion concentration are mainly due to the repulsive force generated by the overlap of the electric double layer and the electrophoresis force generated by the electrophoresis effect. We believe that the factor determining the degree of decline in ion concentration is mainly the degree of overlap of the electric double layer. The initial height h_0 is very sensitive to the effect of the electric double layer overlap because the initial height h_0 affects the width of some of the nanochannel. When the initial height h_0 is reduced, the width of some of the nanochannel is increased. When the width of a part of the nanochannel is increased, the degree of overlap of the electric double layer is lowered, so that the drop is more pronounced after reaching the maximum value.

Our study found that when the initial height h_0 in the Cantor fractal principle was increased from 35 to 45 nm, the peak ion concentration increased by 40% from 1.007 to 1.410 mol/m^3. Therefore, increasing the initial height h_0 is a very efficient method to increase the sensitivity of the microfluidic chip. In the detection of certain tumor cells with particularly low concentrations, we can use this method to significantly increase the concentration of the sample to be tested. This work provides a novel design approach for trace detection equipment.

Effects of fractal step n and the staggered structure on ion enrichment

The purpose is to study the effect of fractal step n and the staggered structure in the Cantor fractal principle on electrokinetic ion enrichment. As shown in Fig. 9, we have designed four different nanochannel wall structures based on the Cantor fractal principle. Figure 9a is a staggered structure with $n=1$. Figure 9b is a unstaggered structure with $n=1$. Figure 9c is a staggered structure with $n=2$. Figure 9d is a unstaggered structure with $n=2$ (the basic structure $S0$). L_0 and h_0 are 200 nm and 40 nm, respectively. A peak concentration curve as shown in Fig. 10 was plotted when a voltage of 1–70 V was applied across the microchannel. It is shown from Fig. 10 that the peak voltages of the staggered structure and the unstaggered structure are almost the same when fractal step n is the same. However, the ion peak concentration of the unstaggered structure is higher than the ion peak concentration of the staggered structure. When the staggered structure is the same and fractal step n increases,

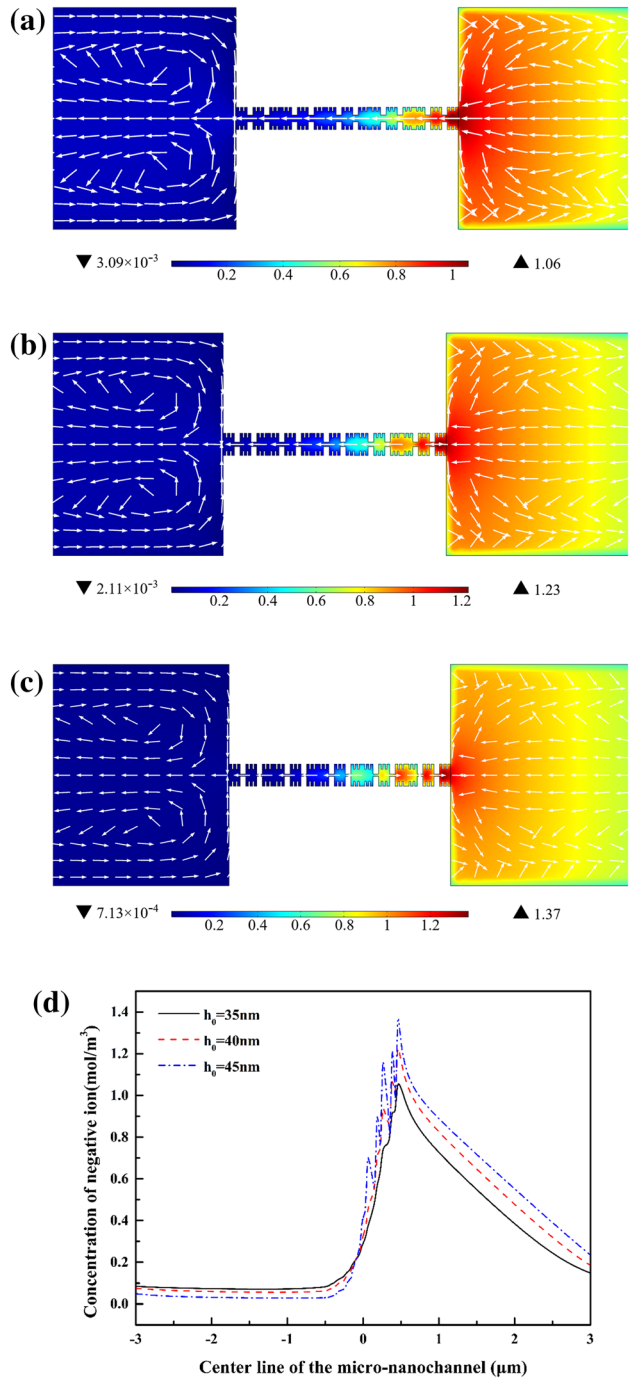

Fig. 8 Ion concentration image of three different initial height h_0 at an applied voltage of 30 V and ion concentration curve at the center line of the micro-nanochannel. **a** h_0=35 nm, **b** h_0=40 nm, **c** h_0=45 nm

the peak ion concentration increases and the peak voltage rises. When fractal step n increases from 1 to 2, the peak ion concentration of the unstaggered structure increases by 20% from 0.960 to 1.152 mol/m^3. To further investigate the effect of fractal step n and the staggered structure on electrokinetic ion enrichment, a concentration plot of four different wall structures with an applied voltage of 28 V is plotted as shown in Fig. 11. Figure 11e shows the ion concentration at the center line of the micro-nano channel. It is seen from Fig. 11a, b (Fig. 11c, d) that the unstaggered structure contains contracted nanochannels when fractal step n is the same. However, the staggered structure does not have a contracted nanochannel. It is precisely because of this contracted nanochannel that the electric double layer overlap is improved. Therefore, the unstaggered nanochannels have a stronger repulsive ability to block ions from passing through the nanochannels. The ion concentration of the enriched region of the unstaggered structure as shown in Fig. 11d is higher than the ion concentration of the enrichment zone of the staggered structure. It can be seen from Fig. 11a, c (Fig. 11b, d) that the number of structural units based on the Cantor fractal principle is significantly increased when the staggered structure is the same and fractal step n is increased from 1 to 2. An increase in the number of Cantor fractal structural units results in an increase in the repulsive force possessed by the surface charge. When fractal step n increases, the ion concentration of the enrichment zone increases remarkably as shown in Fig. 11e. Finally, this study has shown that increasing fractal step n and using the unstaggered structure can increase the ion concentration in the enrichment zone.

Conclusion

To study the nano-electrokinetic ion enrichment in a micro-nanofluidic preconcentrator with nanochannel's Cantor fractal wall structure, a number of different two-dimensional models were designed based on the Poisson–Nernst–Planck equation combined with the Navier–Stokes equation. The effects of the initial length L_0, the initial height h_0, the fractal step n and the staggered structure on the electrokinetic ion enrichment in the Cantor fractal principle are studied. The conclusions are summarized as follows:

1. When the applied voltage is constant and the initial length L_0 decreases, the ion concentration and peak voltage increase. When the initial length L_0 is reduced from 333.33 to 200 nm, the ion peak concentration is increased by 12%.
2. When the applied voltage is constant and the initial height h_0 increases, the ion concentration and peak voltage increase. When the initial height h_0 is increased from 35 to 45 nm, the ion peak concentration is increased by 40%.
3. The ion peak concentration of the unstaggered structure is higher than the ion peak concentration of the staggered structure when the applied voltage and the

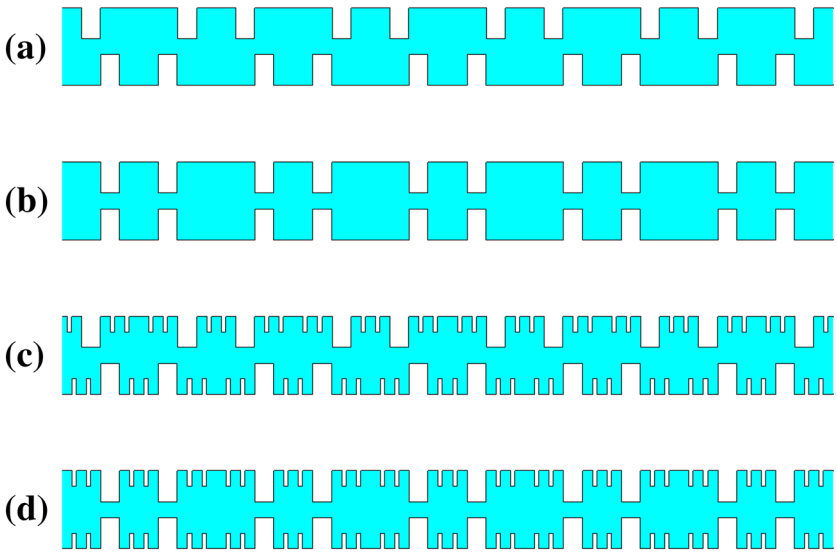

Fig. 9 Design of nanochannel wall structure with different fractal step n and the staggered structure based on Cantor fractal principle. **a** $n=1$, staggered, **b** $n=1$, unstaggered, **c** $n=2$, staggered, **d** $n=2$, unstaggered

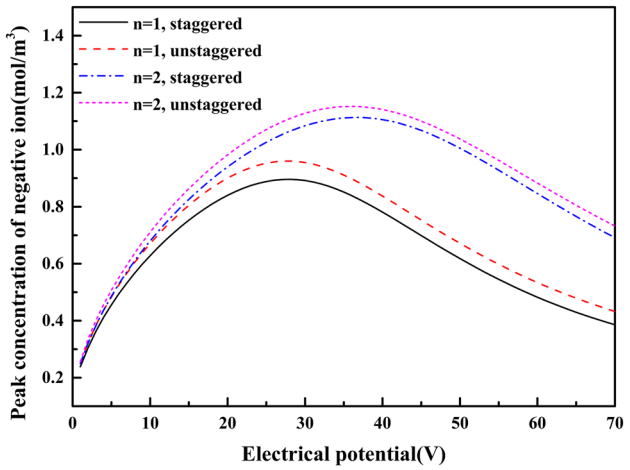

Fig. 10 Ion peak concentration curve for different fractal step n and the staggered structure

fractal step n are constant. When the voltage and staggered structure are constant and the fractal step n is increased, and the ion concentration and peak voltage are increased.

The results show that reducing the initial length L_0, increasing the initial height h_0, increasing the fractal step n and using the unstaggered structure can greatly increase the concentration of electrokinetic ion enrichment based on the Cantor fractal principle. This work provides a novel approach to ultra-low concentration molecular detection, improved micro-nanofluidic chip sensitivity and trace material determination. It provides a theoretical basis for the design of high precision measuring equipment.

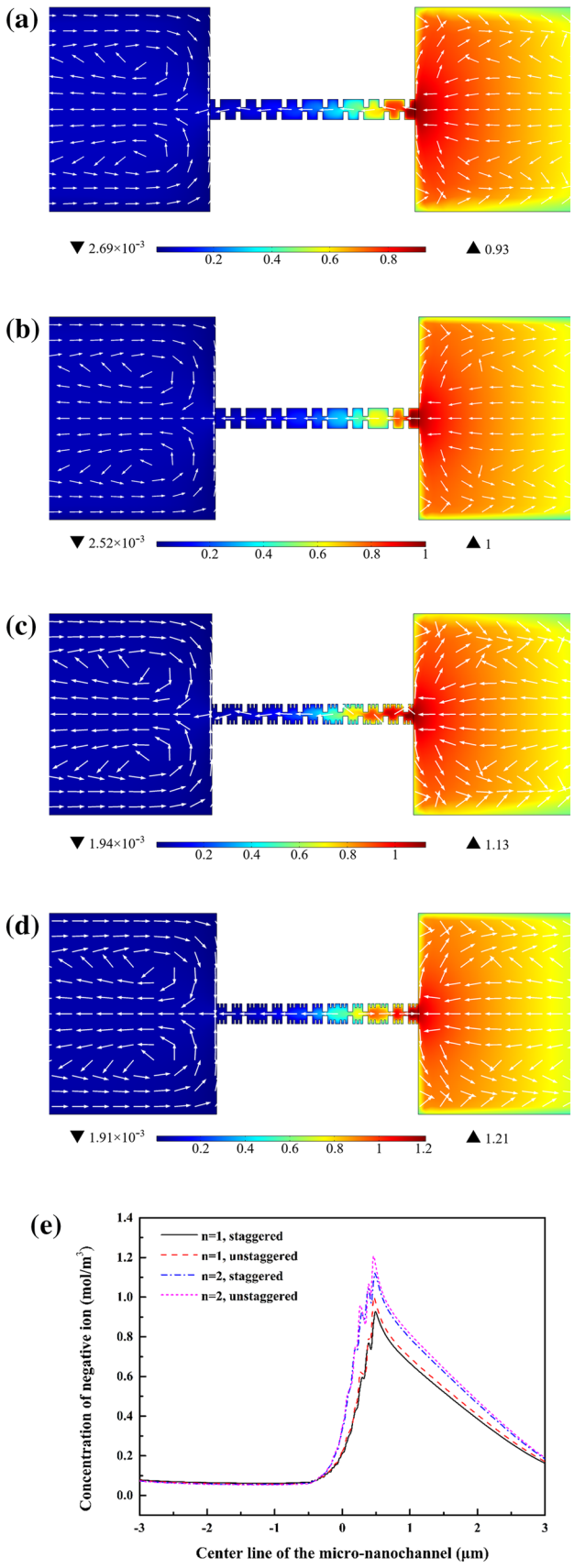

Fig. 11 Ion concentration image of different fractal step n and the staggered structure at an applied voltage of 28 V and ion concentration curve at the center line of the micro-nanochannel. **a** $n=1$, staggered, **b** $n=1$, unstaggered, **c** $n=2$, staggered, **d** $n=2$, unstaggered

Acknowledgements This work was supported by The Key Project of Department of Education of Liaoning Province (JZL201715401), Liaoning Province BaiQianWan Talent Project. We sincerely thank Prof. Chong Liu for his kind guidance.

Compliance with ethical standards

Conflict of interest The authors declare no conflicts of interest.

References

Ali M, Khan WA, Irfan M et al (2019) Computational analysis of entropy generation for cross-nanofluid flow. Appl Nanosci. https://doi.org/10.1007/s13204-019-01038-w

Amoyav B, Benny O (2018) Controlled and tunable polymer particles' production using a single microfluidic device. Appl Nanosci 8:905–914

Cabodi M, Turner SWP, Craighead HG (2002) Entropic recoil separation of long DNA molecules. Anal Chem 74(20):5169–5174

Chen Y, Fu P, Zhang C et al (2010) Numerical simulation of laminar heat transfer in microchannels with rough surfaces characterized by fractal Cantor structures. Int J Heat Fluid Flow 31(4):622–629

Daiguji H, Yang P, Majumdar A (2004) Ion transport in nanofluidic channels. Nano Lett 4(1):137–142

Eijkel JCT, Van Den Berg A (2005) Nanofluidics: what is it and what can we expect from it? Microfluid Nanofluid 1(3):249–267

Gao H, Xie MR, Liu JJ et al (2018) Electrokinetic stacking on paper-based analytical device by ion concentration polarization with ion exchange membrane interface. Microfluid Nanofluid 22(5):50

Gong L, Ouyang W, Li Z et al (2018) Direct numerical simulation of continuous lithium extraction from high Mg2 +/Li + ratio brines using microfluidic channels with ion concentration polarization. J Membr Sci 556:34–41

Hasham AA, Abedini A, Jatukaran A et al (2018) Visualization of fracturing fluid dynamics in a nanofluidic chip. J Petrol Sci Eng 165:181–186

Jia M, Kim T (2014) Multiphysics simulation of ion concentration polarization induced by nanoporous membranes in dual channel devices. Anal Chem 86(15):7360–7367

Jia H, Li Z, Liu C et al (2010) Ultrasensitive detection of microRNAs by exponential isothermal amplification. Angew Chem Int Ed 49(32):5498–5501

Kim SJ, Han J (2008) Self-sealed vertical polymeric nanoporous-junctions for high-throughput nanofluidic applications. Anal Chem 80(9):3507–3511

Kim SJ, Ko SH, Kang KH et al (2010) Direct seawater desalination by ion concentration polarization. Nat Nanotechnol 5(4):297

Lee JH, Chung S, Kim SJ et al (2007) Poly (dimethylsiloxane)-based protein preconcentration using a nanogap generated by junction gap breakdown. Anal Chem 79(17):6868–6873

Li M, Anand RK (2016) Recent advancements in ion concentration polarization. Analyst 141(12):3496–3510

Lin CC, Hsu JL, Lee GB (2011) Sample preconcentration in microfluidic devices. Microfluid Nanofluid 10(3):481–511

Lin CY, Yeh LH, Siwy ZS (2018) Voltage-induced modulation of ionic concentrations and ion current rectification in mesopores with highly charged pore walls. J Phys Chem Lett 9(2):393–398
Liu L, Xie MR, Chen YZ et al (2019) Simultaneous electrokinetic stacking and separation of anionic and cationic species on a paper fluidic channel. Lab Chip 19(5):845–850
MacDonald BD, Gong MM, Zhang P et al (2014) Out-of-plane ion concentration polarization for scalable water desalination. Lab Chip 14(4):681–685
Movahed S, Li D (2011) Electrokinetic transport through nanochannels. Electrophoresis 32(11):1259–1267
Mozaffari S, Tchoukov P, Mozaffari A et al (2017) Capillary driven flow in nanochannels–application to heavy oil rheology studies. Colloids Surf, A 513:178–187
Plecis A, Schoch RB, Renaud P (2005) Ionic transport phenomena in nanofluidics: experimental and theoretical study of the exclusion-enrichment effect on a chip. Nano Lett 5(6):1147–1155
Pu Q, Yun J, Temkin H et al (2004) Ion-enrichment and ion-depletion effect of nanochannel structures. Nano Lett 4(6):1099–1103
Rissin DM, Kan CW, Campbell TG et al (2010) Single-molecule enzyme-linked immunosorbent assay detects serum proteins at subfemtomolar concentrations. Nat Biotechnol 28(6):595
Shi YZ, Xiong S, Zhang Y et al (2018a) Sculpting nanoparticle dynamics for single-bacteria-level screening and direct binding-efficiency measurement. Nat Commun 9(1):815
Shi Y, Xiong S, Chin LK et al (2018b) Nanometer-precision linear sorting with synchronized optofluidic dual barriers. Sci Adv 4(1):eaao0773
Silber-Li ZH, Zheng X, Kong GP et al (2012) Vortices in micro/nano channel flows. WIT Trans Eng Sci 74:533–545
Srinivasacharya D, Surender O (2015) Effect of double stratification on mixed convection boundary layer flow of a nanofluid past a vertical plate in a porous medium[J]. Appl Nanosci 5(1):29–38
van der Heyden FHJ, Bonthuis DJ, Stein D et al (2007) Power generation by pressure-driven transport of ions in nanofluidic channels. Nano Lett 7(4):1022–1025
Wang YC, Han J (2008) Pre-binding dynamic range and sensitivity enhancement for immuno-sensors using nanofluidic preconcentrator. Lab Chip 8(3):392–394
Wang Y, Pant K, Chen Z et al (2009) Numerical analysis of electrokinetic transport in micro-nanofluidic interconnect preconcentrator in hydrodynamic flow[J]. Microfluid Nanofluid 7(5):683
Wang J, Xu Z, Li Y et al (2013) Nanopore density effect of polyacrylamide gel plug on electrokinetic ion enrichment in a micro-nanofluidic chip. Appl Phys Lett 103(4):043103
Wang G, Yang F, Zhao W et al (2016a) On micro-electrokinetic scalar turbulence in microfluidics at a low reynolds number. Lab Chip 16(6):1030–1038
Wang J, Liu C, Xu Z (2016b) Electrokinetic ion transport in confined micro-nanochannel. Electrophoresis 37(5–6):769–774
Whitesides GM (2006) The origins and the future of microfluidics. Nature 442(7101):368
Wu D, Steckl AJ (2009) High speed nanofluidic protein accumulator. Lab Chip 9(13):1890–1896